Quick X-ray reflectivity of spherical samples

Krassimir Stoev,[1,a] and Kenji Sakurai[2,3]
[1]*AECL – Chalk River Laboratories, Chalk River, Ontario, Canada*
[2]*University of Tsukuba, 1-1-1 Tennodai, Tsukuba, Ibaraki, Japan*
[3]*National Institute for Materials Science, 1-2-1 Sengen, Tsukuba, Ibaraki, Japan*

(Received 12 February 2013; accepted 14 February 2013)

Recently, a new experimental setup for quick X-ray reflectivity (q-XRR) measurements was proposed, which is based on simultaneous recording of an X-ray reflectivity curve over all angles of interest. This new setup for q-XRR allows measurements to be done within seconds, thus permitting studies of the time evolution of chemical, thermal, and mechanical changes at the surfaces and interfaces of different materials. Since the q-XRR measurement setup utilizes an extended X-ray source and detector, it is important to develop models and to account for the following two effects: (i) diffuse scattering associated with different points of the source and (ii) sample curvature. Models accounting for both effects are presented, and their influences on interpretation of the q-XRR measurement results are discussed. © *2013 International Centre for Diffraction Data*. [doi:10.1017/S0885715613000134]

Key words: X-ray reflectivity, diffuse scattering, sample curvature

I. INTRODUCTION

X-ray reflectivity is a non-destructive testing technique used to investigate the structure of surfaces, buried interfaces, thin films, and multi-layers. Classical X-ray reflectivity is a relatively slow technique, with a typical time for one scan of the order of hours. Recently, a new experimental setup for quick X-ray reflectivity (q-XRR) measurements was proposed (Sakurai and Mizusawa, 2007; Sakurai *et al.*, 2007a, 2007b; Naudon *et al.*, 1989; Chihab and Naudon, 1992; Naudon, 1992; Albouy and Valerio, 1997; Koppel, 1997; Niggemeier *et al.*, 1997), which is based on simultaneous recording of the X-ray reflectivity curve over all angles of interest. The new setup for q-XRR will allow measurements to be done within seconds, thus permitting studies of the time evolution of chemical, thermal, and mechanical changes at the surfaces and interfaces of different materials. Since the q-XRR measurement setup utilizes an extended X-ray source, it will be important to develop models and to account for two effects:

- Both specular reflection and diffuse scattering associated with different points of the source can reach each pixel of the detector.
- Sample curvature (for example, surface of a liquid sample) will lead to changes in the recorded X-ray reflectivity curve in comparison to a flat sample.

Models accounting for both effects will be presented, and their influence on interpretation of the measurement results from q-XRR will be discussed. For spherical samples at glancing incidence, because the source is very close to the sample, one has to consider strong aberrations in forming the source image. Owing to strong aberration effects, the image of the line source will not be a line, but will have a complex 3D shape, i.e., it will be blurred. Generally speaking, there will be two images formed: one by the rays parallel to the incidence plane (tangential image); and one by the rays perpendicular to the incidence plane (sagittal image). Both concave and convex spherical surfaces of the sample will be considered, and the contribution of sample curvature to the measured signal will be evaluated by means of computer simulations. Such simulations are very important for interpretation of the results from q-XRR measurements, because diffuse scattering and sample curvature effects can cause changes in the shape of the X-ray reflectivity curve that are similar to the changes introduced by the sample structural parameters such as density, roughness, layer thickness, etc.

II. MEASUREMENTAL

A schematic of the q-XRR setup is shown in Figure 1. The real experimental setup used for the modeling done in this paper is shown in the inset in Figure 1. The linear source has a height of around 10 mm, which at source-to-slit distance (L_{SK}) of 270 mm provides incident angles in the range 0–37 mrad on the sample. The source emits the Cu$K\alpha$ line (8.047 keV). The slit-to-detector distance is 1800 mm. The slit height (H_K) is 30 μm, and the detector is a linear pixel array (1024 pixels, with detector pixel height $D_H = 50\ \mu$m). This corresponds to a maximum reflection angle of 28 mrad.

For the purpose of this work, the words "sample" and "mirror" will both be used for describing the reflector. To facilitate comparison of the results from different models, one and the same sample was used for all calculations. A multi-layer sample (10 bi-layers of 3-nm Ni/3-nm C, on a Si substrate) was selected, because it produces X-ray reflectivity scans that have both a Bragg-peak and side-lobes (fringes).

III. MODELING THE EFFECT OF DIFFUSE SCATTERING

Owing to the use of an extended source and detector in the q-XRR, each detector pixel will see the specular reflection from

[a]Author to whom correspondence should be addressed. Electronic mail: stoevk@aecl.ca

https://doi.org/10.1017/S0885715613000134 Published online by Cambridge University Press

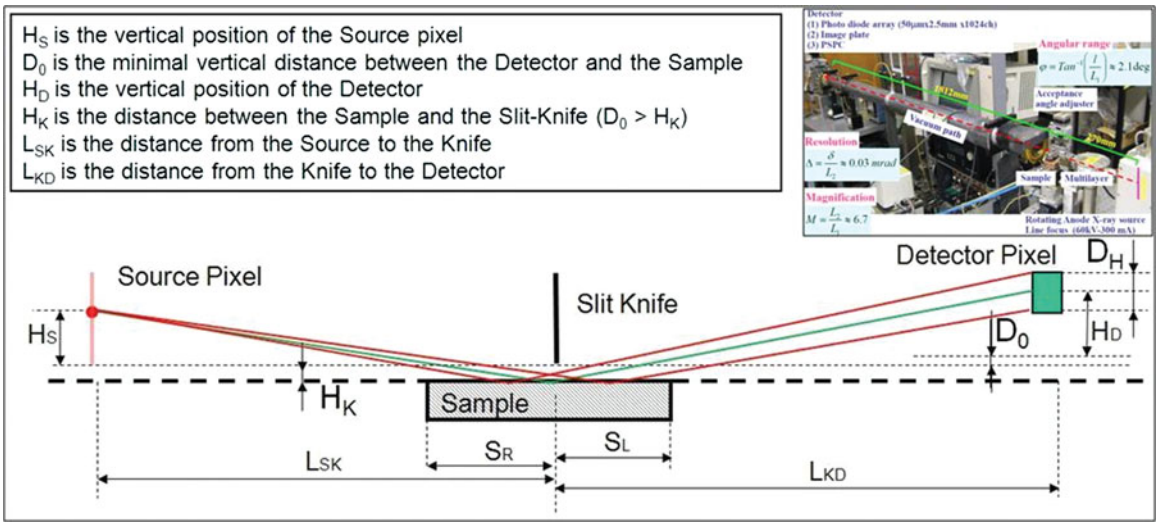


Figure 1. Schematic of the q-XRR setup.

the corresponding source point plus the diffuse scattering from all source points, i.e. the diffuse scattering contribution has to be integrated over all incident angles φ_{In} for each specular angle φ_{Out}. Preliminary results on the contribution of diffuse scattering to the q-XRR scans for a polished surface and a thin film sample were reported by the authors in a previous publication (Stoev *et al.*, 2009). Calculations were done using DS2D software (Mizusawa *et al.*, 2003) and TRDS software (Stepanov, 2012). The results from modeling the multi-layered sample are shown in Figure 2 for different combinations of vertical roughness *S*, correlation length *L*, and Hurst parameter *H*.

As can be seen, the integrated diffuse scattering does not change significantly the shape of the q-XRR curve up to angles of 15 mrad. Above that angle, the amplitude of the side-lobes is reduced, but their position and width are not changed. Unlike classical scanning X-ray reflectivity, the dynamic range of the detectors for q-XRR is not so wide (usually on the order of 4–4.5 decades for 16-bit digitization). If only the region below 15 mrad is used for fitting and extracting of sample parameters from experimental q-XRR scans, there is no need to include the contribution of diffuse scattering in the modeling function. These results are similar to the ones previously published (Stoev *et al.*, 2009).

IV. MODELING THE EFFECTS OF X-RAY BEAM DIVERGENCE

The sample curvature will generally have the same effect on the reflectivity curve as introducing beam divergence. The effects of X-ray beam divergence for the classical X-ray reflectivity setup (with slits/collimators at both source and detector) were modeled with RefleX6 software (Stoev *et al.*, 1997; Stoev and Sakurai, 2011).

The results are presented in Figure 3, and can be used for comparison with the results of modeling the q-XRR setup with curved samples. As can be seen, the increase in X-ray beam divergence leads to:

- Reduction in the intensity and increase of the width of the Bragg peak, with practically no change in the position of the Bragg peak.
- Significant change in the slope of the X-ray reflectivity curve around the critical angle of total reflection.
- Significant change in the intensity and shift in the position of the high-frequency fringes (also known as side-lobes). These changes are observed both around the Bragg peak and in the region around the critical angle of total reflection.

V. MODELING SAMPLE CURVATURE EFFECTS FOR CONVEX SAMPLES

For comparison only, the previously developed software RefleX6 (Stoev *et al.*, 1997; Stoev and Sakurai, 2011) was used to model the effects of the radius of curvature for convex samples on the shape of the q-XRR reflectivity curves. As discussed in Stoev and Sakurai (2011), there are two preferred ways to perform such modeling. The first approach is to use a 2D numerical integration of X-ray reflectivity over the whole sample for each detector point. The sample is divided into N_S sub-intervals and, for each detector pixel and each sample sub-interval, the corresponding source point and reflection angle are calculated. Corrections are made for the shadowing effects because of the knife-slit, self-shadowing because of the mirror curvature, and for the finite sample size. This model correctly accounts for the changing reflection angle from sub-interval to sub-interval and for the detector acceptance angle for each sub-interval. Results from this model are shown in Figure 4.

Although very simple and easy to use, the model described above has some disadvantages, and more specifically it assumes a cylindrical sample, not a spherical sample. In order to overcome this deficiency, another model was proposed (Stoev and Sakurai, 2011), which accounts for the 3D shape of the spherical mirror. This is done by using the source image rather than the source itself. For spherical samples at glancing incidence, because the source is very close to the sample, there are very strong aberration effects in forming the source image. Discussion on this subject can be found in Bridou (1994). Two images will be formed: a tangential image (formed by the rays parallel to the incidence plane); and a sagittal image (formed by the rays perpendicular to the incidence plane). This will lead to blurring of the image, i.e. the image of a line-source will not be a line, but will have a complex 3D shape. At

https://doi.org/10.1017/S0885715613000134 Published online by Cambridge University Press

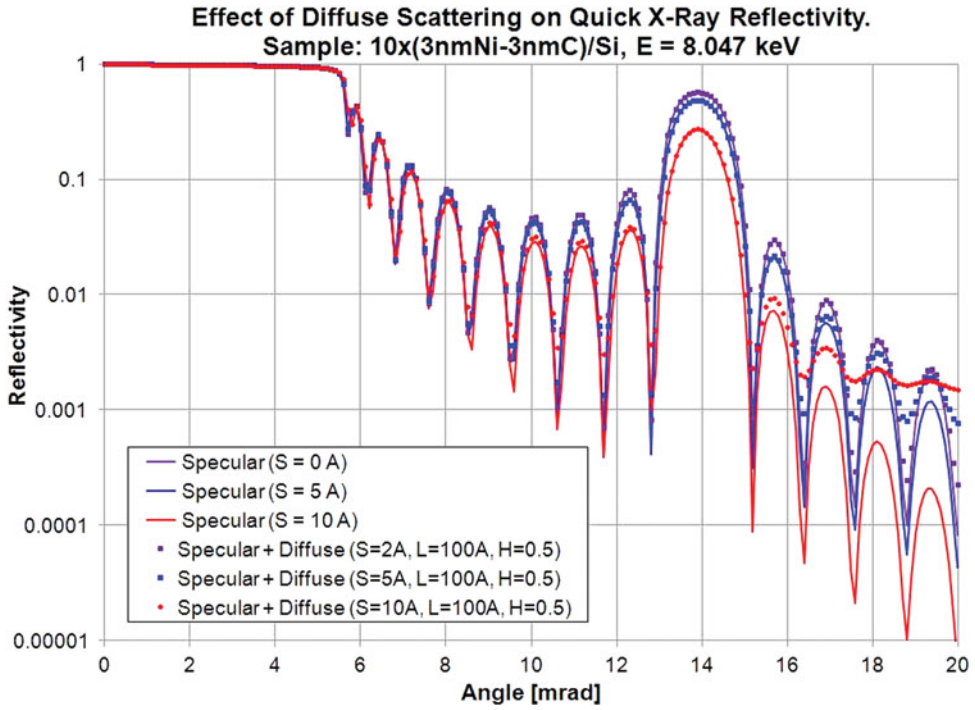


Figure 2. Effect of diffuse scattering on q-XRR.

glancing incidence, the position of the sagittal image does not change significantly with the incident angle. On the other hand, the position of the tangential image depends very strongly on the incident angle. The calculation of the reflectivity from a 3D spherical mirror is again based on numerical integration. The source is divided into small sub-sections, the sample is also divided in N_S sub-intervals, and for each source sub-section and sample sub-section, the reflection angle, the tangential image, and the corresponding detector pixel are determined, and the calculated intensity is added to the total intensity for the corresponding detector pixel. For each source sub-section and sample sub-section, the position of the tangential image is used to calculate the correction factor (i.e., correction for different angular density of beam energy because of different divergence for the beams reflected from a flat and convex sub-interval). Results from calculations based on the 3D model are shown in Figure 5. There is no significant difference between the two models for convex samples (see Figures 4 and 5), mainly because convex mirrors always produce beams that have larger divergence than the beams produced by flat mirrors,

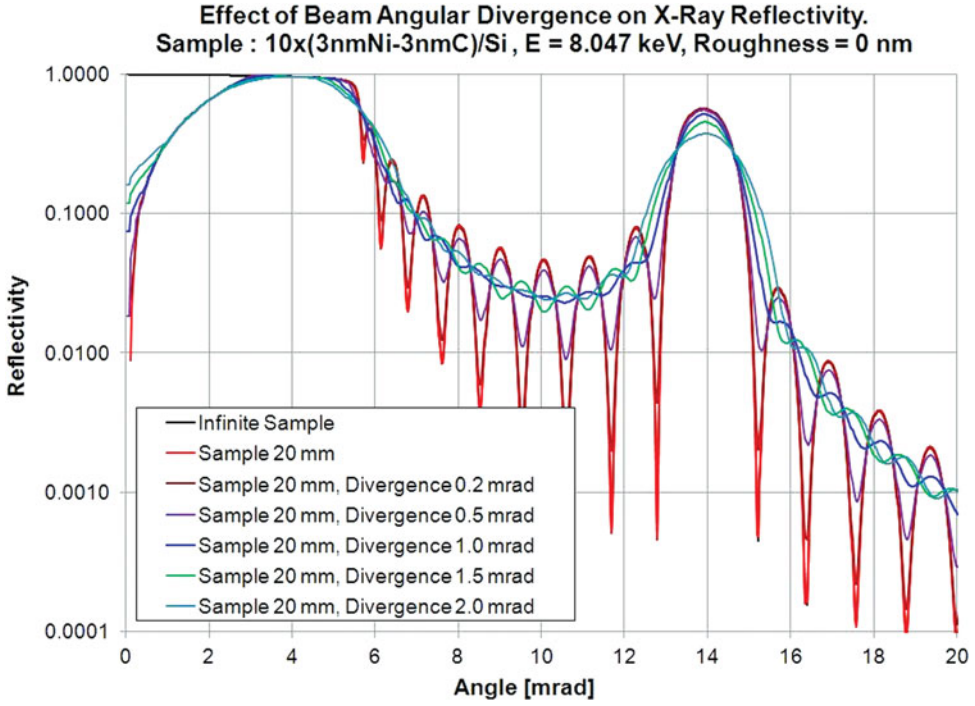


Figure 3. Effect of beam divergence in classical X-ray reflectivity.

https://doi.org/10.1017/S0885715613000134 Published online by Cambridge University Press

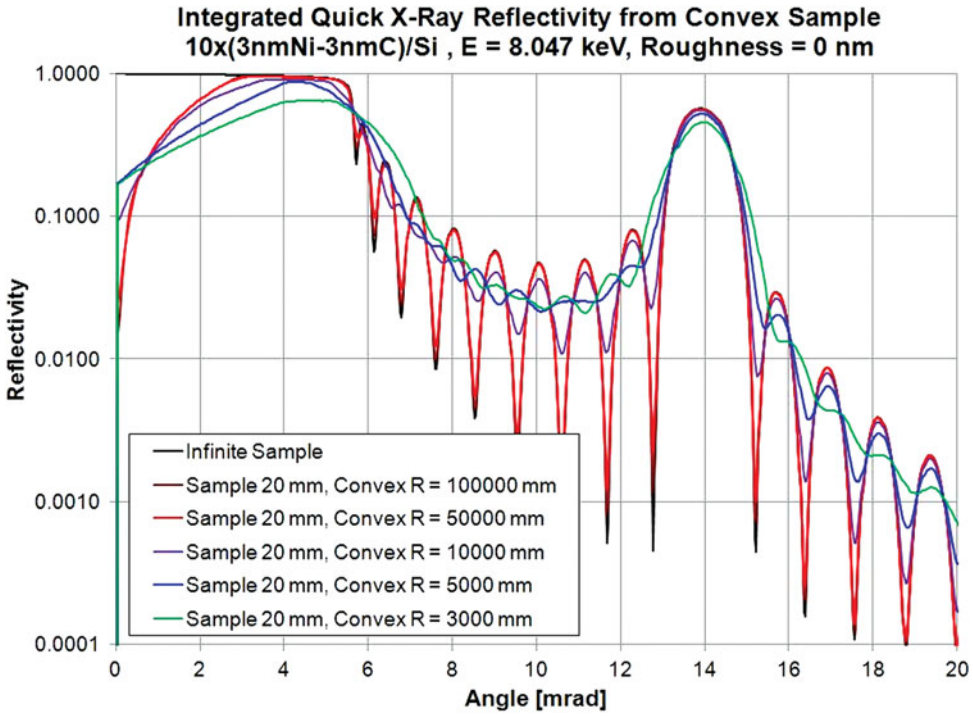


Figure 4. Effect of sample curvature on q-XRR scans (numerical integration).

i.e. there will be a slight reduction of the angular density of beam energy for convex mirrors when compared with flat mirrors.

VI. MODELING SAMPLE CURVATURE EFFECTS FOR CONCAVE SAMPLES

The modeling setup for the q-XRR scans from a concave mirror is shown in Figure 6. In this case, several additional shadowing effects have to be considered:

- For concave mirrors, it is possible to have sections of the line-source or of the detector that are completely shadowed, i.e. from which no point of the mirror surface is visible. The highest point for these sections is defined as the intersection point of the source (or the detector) with the line through knife-end and mirror-end. For example, in Figure 6, all the points in the brown sections of the source will not "see" any point of the top-surface of the mirror.
- Self-shadowing of the mirror will occur when some parts of the mirror are blocking other parts of the mirror from seeing

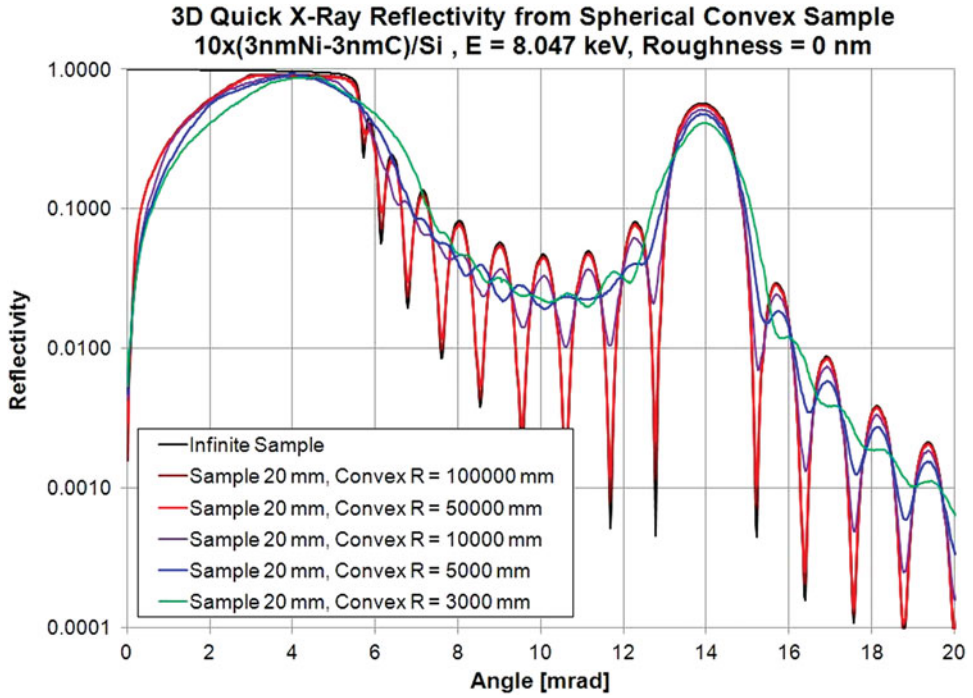


Figure 5. Effect of sample curvature on q-XRR scans (3D model).

https://doi.org/10.1017/S0885715613000134 Published online by Cambridge University Press

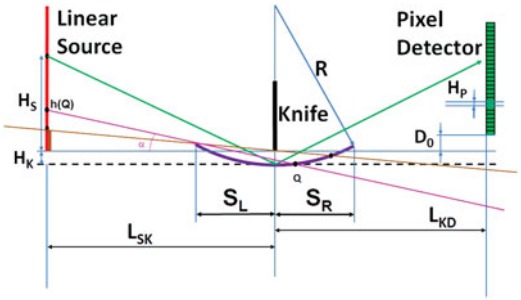


Figure 6. q-XRR setup for a concave mirror.

the rays from the source (or to the detector). For example in Figure 6, all source points below $h(Q)$ are blocked by the left end of the mirror from seeing the parts of the mirror to the left of point Q.

Again, two approaches were considered: 2D numerical integration over a cylindrical concave mirror and 3D numerical integration while accounting for changes in the position of the tangential image. Both methods were implemented in a revised version of the RefleX6 software.

The 2D numerical integration is based on dividing the sample into N_S sub-intervals and, for each detector pixel and each sample sub-interval, calculating the corresponding source point and reflection angle. Corrections are made for all shadowing effects and for the finite sample size. Results from this model are shown in Figure 7. This model correctly accounts for the changing reflection angle from sub-interval to sub-interval, and for the acceptance angle for each sub-interval. The main problem with this model is that it assumes that each mirror sub-section is a flat mirror, i.e. it does not account for the additional beam divergence (or convergence) introduced by the curvature of the mirror sub-section.

For a concave mirror, we can have discontinuities in the tangential image. This was partially discussed in Bridou (1994). The sagittal and the tangential image points are introduced for convenience only, and do not represent the true "blurred" image as formed by complete ray-tracing of the optical system. The position of the sagittal and tangential image points can be calculated using standard formulas (also known as the Coddington equations):

$$\frac{1}{d_0}+\frac{1}{d_S}=\frac{2.\sin(\theta)}{R},$$
$$\frac{1}{d_0}+\frac{1}{d_T}=\frac{2}{R\sin(\theta)}.$$

The sign convention is as follows: d_0, d_S, d_T, and R are positive to the left of the vertex point, and negative to the right of the vertex point, while θ is always positive. For small angles θ, the sagittal image position d_S does not depend significantly on θ, and its value is close to d_0, while tangential image position d_T depends strongly on θ. There will be an angle θ, for which $d_T=\infty$, i.e. we will have a discontinuity in the tangential image. This corresponds to having parallel beams, for which no image is formed. Again, these formulas are only an approximation, because they do not consider that many parts of the mirror are involved in the creation of the image.

An illustration of this problem is shown in Figure 8, for the case of a concave mirror with a curvature radius of 30 m. This mirror transforms the red part of the source into the purple part of the tangential image (image is "above" the mirror), while the green part of the source is transformed by the mirror into the yellow part of the tangential image (i.e., image is "below" the mirror). The source point between the red and the green part of the source does not produce an image, it produces a parallel beam. The tangential image for the case described above

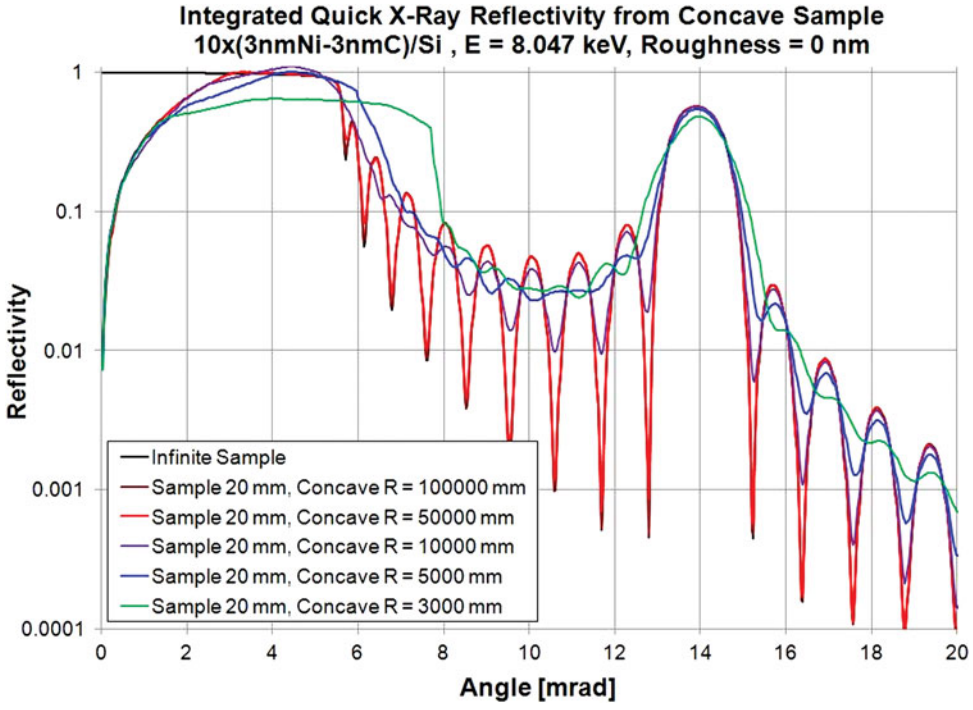


Figure 7. Integrated 2D q-XRR reflectivity for a concave mirror.

https://doi.org/10.1017/S0885715613000134 Published online by Cambridge University Press

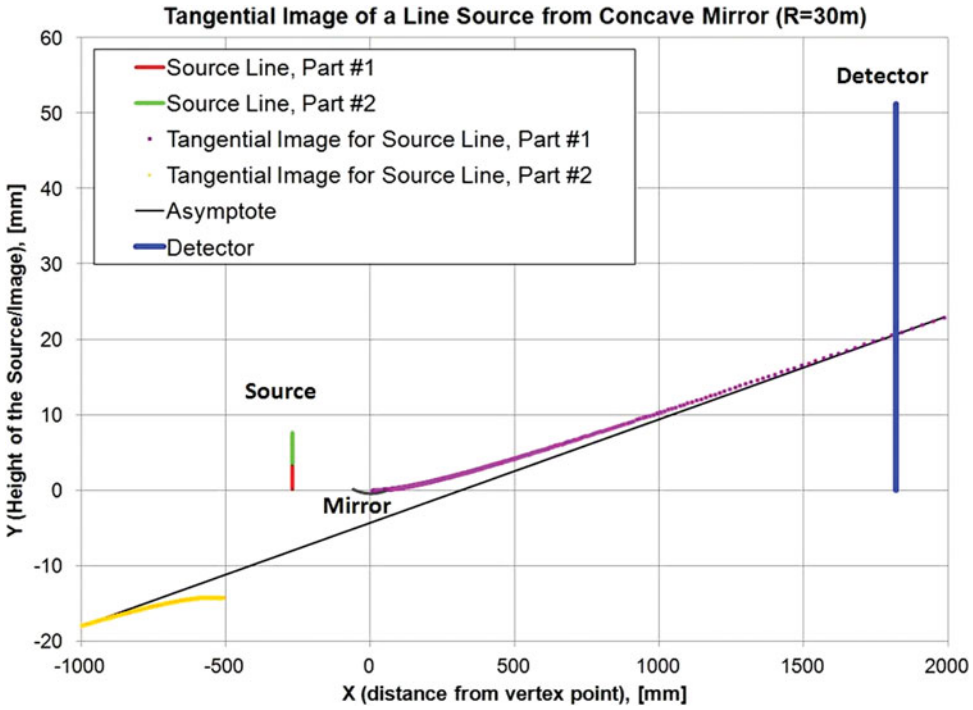


Figure 8. Discontinuities in the tangential image.

was calculated based on the rays passing through the ends of the mirror.

Another problem is that different parts of the mirror form beams with different divergence, i.e. different tangential images. Also, there are several effects that contribute to the energy density of the beam on the detector pixels for the case of flat and convex mirrors:

- Different parts of the mirror will contribute to each detector pixel.
- Different mirror lengths will correspond to the pass-through beam for each source point.
- A different number of detector pixels will be illuminated by the pass-through beam for each source point.

All these effects have to be considered simultaneously when modeling q-XRR scans of concave mirrors. This is done by evaluating the "illuminated" parts of the detector for each source point and each mirror subsection, for both flat (H_F) and concave (H_C) mirrors, as illustrated in Figure 9. The correction factor (H_F/H_C) is used to normalize final results. In addition to this correction, the results have to be normalized in such a way as to ensure that integration of a flat mirror, by following the procedure for integration and

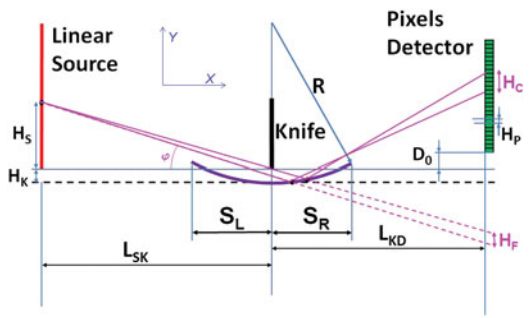


Figure 9. "Illuminated" parts of the detector for flat and concave mirrors.

correction of a concave mirror will produce the same results as the theoretical reflectivity of a limited flat sample.

It should be noted that, for specific cases, H_C could become very close to zero (i.e., the mirror sub-section generates a tangential image onto the detector line, as shown in Figure 8). In these cases, the correction factor becomes very large. To avoid such cases, the maximum value of the correction factor was restricted based on the sizes of the source pixels and detector pixels, and the "nominal" beam spread from a flat sub-section. Even with this restriction, for some values of radius of curvature R and nominal reflection angle θ, there will be large uncertainties in the corrected results, as shown in Figure 10.

Results from the calculation of the q-XRR scans from concave mirrors with different radii of curvature as per the above described procedure are shown in Figure 10. The 3D q-XRR scans are similar to the 2D integrated q-XRR scans presented in Figure 7, but the difference is bigger for the case of concave mirrors than that for convex mirrors (see Figures 4 and 5). This can be attributed to the larger beam divergence from each section for the concave mirrors in comparison to the convex mirrors, i.e. larger changes and discontinuities in the position of the tangential image for the case of a concave mirror.

Generally speaking, the effects of the sample curvature on the shape of the q-XRR scans for concave mirrors are similar to those for convex mirrors. Usually, these effects are significant when the radius curvature, R, is <10 m, and are very similar to the effects of X-ray beam angular divergence in classical X-ray reflectivity (see Figure 3):

- Reduction in the intensity and increase in the width of the Bragg peak, accompanied with small change in the position of the Bragg peak.
- Significant change in the shape and the slope of the q-XRR curve around the critical angle of total reflection.
- Significant change in the intensity and shift in the position of the high-frequency fringes (or side-lobes). These changes

https://doi.org/10.1017/S0885715613000134 Published online by Cambridge University Press

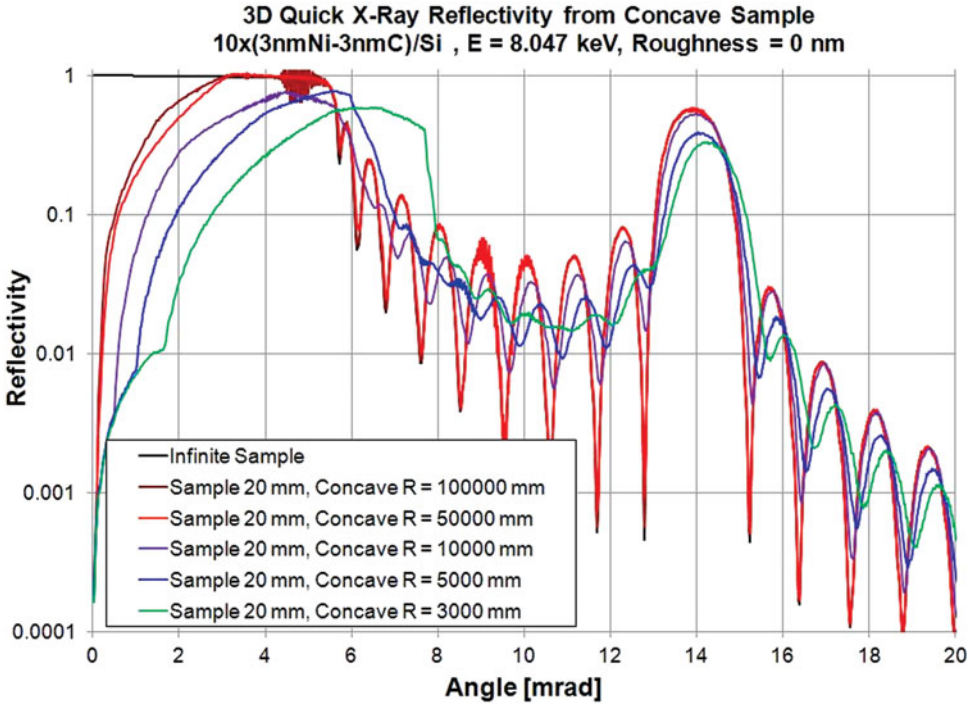


Figure 10. Calculated 3D q-XRR reflectivity for a concave mirror.

are observed both around the Bragg peak and around the critical angle of total reflection.

VII. CONCLUSION

The recently developed q-XRR technique offers unique capabilities for studying fast processes at the surface and interface of nano-scale materials, such as the time evolution of chemical, thermal, and mechanical changes at the surface and the interface of different objects or materials. The current study was directed at determining the contribution of diffuse scattering and sample curvature to the measured signal from a q-XRR setup. In some cases, the integrated diffuse scattering can significantly influence the shape of the recorded reflectivity curves with the q-XRR setup. The effects of the sample curvature on the shape of the reflectivity curve measured with the q-XRR setup are even more severe, manifested as changes in the position and width of the Bragg peak and/or side-lobes. In order to obtain reliable data from the q-XRR measurements, the existing models for description of X-ray reflectivity curves must be modified to include the contribution of diffuse scattering and to account for sample curvature.

Albouy, P. and Valerio, P. (**1997**). "A motionless X-ray reflectometer for air/liquid interface based on Naudon's design: example of application", Supromol. Sci. **4**, 191–194.

Bridou, F. (**1994**). "Curvature effect in grazing X-ray reflectometry", J. Phys. III France **4**, 1513–1522.

Chihab, J. and Naudon, A. (**1992**). "Possibilites de mesure quantitative avec un appareilage de reflectometrie X utilisant le mode angulaire dispersive," J. Phys. III (France), **2**, 2291–2300.

Koppel, L. N. (**1997**). "X-ray thickness gauge", US Patent No. 5619548.

Mizusawa, M., Stoev, K., and Sakurai, K. (**2003**). "Analysis of surface X-ray scattering from synthetic quartz mirror", 2002 Photon Factory Activity Report Part B, 20, 64.

Naudon, A. (**1992**). "Mode mini pour la reflectrometrie,"Analusis (France), **18**, I22.

Naudon, A., Chihab, J., Goudeau, P., and Mimault, J. (**1989**). "New apparatus for grazing X-ray reflectometry in the angle-resolved dispersive mode," J. Appl. Cryst., **22**, 460–464.

Niggemeier, U., Lischka, K., Plotz, W. M., and Holy, V. (**1997**). "X-ray Reflectometer for the Diagnostics of Thin Films During Growth," J. Appl. Cryst., **30**, 905–908.

Sakurai, K. and Mizusawa, M. (**2007**). Japanese Patent No. 3903184.

Sakurai, K., Mizusawa, M., and Ishii, M. (**2007a**). "Recent Novel X-ray Reflectivity Techniques: Moving Towards Quicker Measurement to Observe Changes at Surface and Buried Interfaces," Trans. MRS Japan, **32**, 181–186.

Sakurai, K., Mizusawa, M., Ishii, M., Kobayashi and Imai, S. (**2007b**). "Instrumentation for X-ray reflectivity in micro area: present status and future outlook", J. Phys., Conf. Ser. U.K., **83**, 012001.

Stepanov, S. (**2012**). "TRDS On-Line Calculation Tool for X-ray Diffuse Scattering", available online at http://sergey.gmca.aps.anl.gov/TRDS_sl.html

Stoev, K., Knoth, J., and Schwenke, H. (**1997**). "X-ray reflectivity simulation software," in 7th German–Japanese Workshop on Chemical Information, April 10–12, 1997, Nara, Japan (http://inaba.nims.go.jp/G-J/report/stoev.html).

Stoev, K., Samson, V., Mizusawa, M., and Sakurai, K. (**2009**). "Calculation of diffuse scattering in quick X-ray reflectometry", in *45 Annual Conference on X-ray Chemical Analysis*, November 5–6, 2009, Osaka, Japan.

Stoev, K. and Sakurai, K. (**2011**). "Aberration effects in quick X-ray reflectivity of curved samples", IOP Conf. Ser.: Mater. Sci. Eng. **24**, 012014.

https://doi.org/10.1017/S0885715613000134 Published online by Cambridge University Press